Contemporary Mathematics
Volume **218**, 1998
B 0-8218-0988-1-03006-5

A Fictitious Domain Method with Distributed Lagrange Multipliers for the Numerical Simulation of Particulate Flow

Roland Glowinski, Tsorng-Whay Pan, Todd I. Hesla, Daniel D. Joseph, and Jacques Periaux

1. Introduction

The main goal of this article, which generalizes [**4**] considerably, is to discuss the *numerical simulation* of *particulate flow* for mixtures of *incompressible viscous fluids* and *rigid particles*. Such flow occurs in liquid/solid *fluidized beds, sedimentation*, and other applications in Science and Engineering. Assuming that the number of particles is sufficiently large, those simulations are useful to adjust parameters in the *homogenized models* approximating the above *two-phase flow*.

From a *computational* point of view, the methodology to be discussed in this article combines *distributed Lagrange multipliers* based *fictitious domain methods*, which allow the use of *fixed structured finite element grids* for the fluid flow computations, with *time discretizations* by *operator splitting à la Marchuk-Yanenko* to decouple the various computational difficulties associated to the simulation; these difficulties include *collisions* between particles, which are treated by *penalty* type methods. After validating the numerical methodology discussed here by comparison with some well documented *two particle - fluid flow* interactions, we shall present the results of two and three dimensional particulate flow simulations, with the number of particles in the range $10^2 - 10^3$; these results include the simulation of a *Rayleigh-Taylor instability* occurring when a sufficiently large number of particles, initially at rest, are positioned regularly over a fluid of smaller density, in the presence of gravity.

The methods described in this article will be discussed with more details (of computational and physical natures) in [**6**]. Actually, ref. [**6**] will contain, also, many references to the work of several investigators, showing that the most popular methodology to simulate particulate flow has been so far the one based on *ALE (Arbitrary Lagrange-Euler)* techniques; these methods are clearly more complicated to implement than those described in this article (particularly on *parallel* platforms).

1991 *Mathematics Subject Classification.* Primary 65M55; Secondary 65M60, 70F99, 76P05.

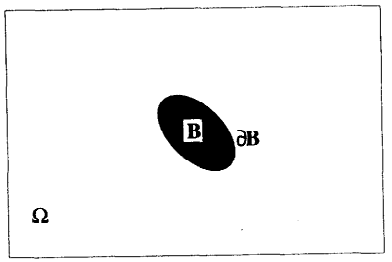

FIGURE 1. The rigid body B and the flow region $\Omega\backslash\bar{B}$

2. A model problem

For simplicity, we shall consider first the motion of a *unique rigid body* B, surrounded by a *Newtonian incompressible viscous fluid*. From a geometrical point of view, the situation is the one depicted in Figure 1.

The rigid body $B(t)(= B)$ is contained in a region $\Omega \subset I\!R^d (d = 2, 3$, in practice). The *fluid flow* is modelled by the following *Navier-Stokes equations* (with obvious and/or classical notation):

$$\rho_f \left[\frac{\partial \mathbf{u}}{\partial t} + (\mathbf{u}\cdot\nabla)\mathbf{u}\right] = \rho_f \mathbf{g} + \nabla\cdot\boldsymbol{\sigma} \text{ in } \Omega\backslash\overline{B(t)}, \tag{1}$$

$$\nabla\cdot\mathbf{u} = 0 \text{ in } \Omega\backslash\overline{B(t)}, \tag{2}$$

$$\mathbf{u}(x,0) = \mathbf{u}_0(x), x \in \Omega\backslash\overline{B(0)}, \text{ with } \nabla\cdot\mathbf{u}_0 = 0, \tag{3}$$

$$\mathbf{u} = \mathbf{g}_0 \text{ on } \Gamma. \tag{4}$$

We remind that for *Newtonian fluids* the *stress tensor* $\boldsymbol{\sigma}$ is defined by

$$\boldsymbol{\sigma} = -p\mathbf{I} + \nu_f(\nabla\mathbf{u} + \nabla\mathbf{u}^t). \tag{5}$$

Assuming that a *no-slip condition* holds on $\partial B(t)$, the *rigid body motion* of $B(t)$, combined with the *incompressibility condition* (2), implies that $\int_\Gamma \mathbf{g}_0\cdot\mathbf{n}d\Gamma = 0$.

For further simplicity, we shall assume that $\Omega \subset I\!R^2$, but there is no basic difficulty to generalize the following considerations to three-dimensional particulate flow. Denoting by $\mathbf{V}$ (resp., ω) the *velocity of the center of mass* G (resp., the *angular velocity*) of the rigid body B, we have for the motion of B the following *Newton's equations*:

$$M\dot{\mathbf{V}} = \mathbf{F} + M\mathbf{g}, \tag{6}$$

$$I\dot{\omega} = T, \tag{7}$$

$$\dot{G} = \mathbf{V}, \tag{8}$$

with the *force* $\mathbf{F}$ and *torque* T, resulting from the *fluid-particle interaction*, given by

$$\mathbf{F} = \int_{\partial B}\boldsymbol{\sigma}\mathbf{n}d\gamma, \tag{9}$$

$$T = \int_{\partial B}(\vec{Gx}\times\boldsymbol{\sigma}\mathbf{n})\cdot\mathbf{e}_3 d\gamma, \tag{10}$$

where, in (10), $\mathbf{e}_3 = \{0,0,1\}$ if we assume that Ω is contained in the plane x_1Ox_2. The no-slip boundary condition mentioned above implies that on ∂B we have

$$\mathbf{u}(x,t) = \mathbf{V}(t) + \boldsymbol{\omega}(t)\times\vec{Gx},\ \forall x \in \partial B(t), \tag{11}$$

with $\boldsymbol{\omega} = \{0,0,\omega\}$. Of course, I is the *moment of inertia* of B, with respect to G.

3. A global variational formulation

We introduce first the following *functional spaces*

$$\begin{aligned} V_{g_0(t)} &= \{\mathbf{v}|\mathbf{v}\in H^1(\Omega\backslash\overline{B(t)})^2,\ \mathbf{v} = \mathbf{g}_0(t) \text{ on } \Gamma\},\\ V_0(t) &= \{\mathbf{v}|\mathbf{v}\in H^1(\Omega\backslash\overline{B(t)})^2,\ \mathbf{v} = 0 \text{ on } \Gamma, \mathbf{v} = \mathbf{Y} + \boldsymbol{\theta}\times\vec{Gx}\\ &\quad \text{on } \partial B, \mathbf{Y}\in I\!R^2,\ \theta\in I\!R\},\\ L^2_0(\Omega\backslash\overline{B(t)}) &= \{q|q\in L^2(\Omega\backslash\overline{B(t)}), \int_{\Omega\backslash\overline{B(t)}} q dx = 0\} \end{aligned}$$

with $\boldsymbol{\theta} = \{0,0,\theta\}$. By application of the *virtual power principle* (ref. [7]) we are led to look for:

$$\mathbf{u}(t)\in V_{g_0(t)}, p\in L^2_0(\Omega\backslash\overline{B(t)}), \mathbf{V}(t)\in I\!R^2, \omega(t)\in I\!R \text{ such that}$$

$$\begin{cases} \rho_f\int_{\Omega\backslash\overline{B(t)}}\frac{\partial\mathbf{u}}{\partial t}\cdot\mathbf{v}dx + \rho_f\int_{\Omega\backslash\overline{B(t)}}(\mathbf{u}\cdot\nabla)\mathbf{u}\cdot\mathbf{v}dx - \int_{\Omega\backslash\overline{B(t)}}p\nabla\cdot\mathbf{v}dx\\ +2\nu_f\int_{\Omega\backslash\overline{B(t)}}\mathbf{D}(\mathbf{u}):\mathbf{D}(\mathbf{v})dx + M(\dot{\mathbf{V}}-\mathbf{g})\cdot\mathbf{Y} + I\dot{\omega}\theta\\ = \rho_f\int_{\Omega\backslash\overline{B(t)}}\mathbf{g}\cdot\mathbf{v}dx,\ \forall\mathbf{v}\in V_0(t),\ \forall\{\mathbf{Y},\theta\}\in I\!R^3, \end{cases} \tag{12}$$

$$\int_{\Omega\backslash\overline{B(t)}} q\nabla\cdot\mathbf{u}(t)dx = 0,\ \forall q\in L^2(\Omega\backslash\overline{B(t)}), \tag{13}$$

$$\mathbf{u} = \mathbf{g}_0 \text{ on } \Gamma, \tag{14}$$

$$\mathbf{u} = \mathbf{V} + \boldsymbol{\omega}\times\vec{Gx} \text{ on } \partial B(t), \tag{15}$$

$$\mathbf{u}(x_0) = \mathbf{u}_0(x),\ \forall x\in\Omega\backslash\overline{B(0)}, \text{ with } \nabla\cdot\mathbf{u}_0 = 0, \tag{16}$$

$$\mathbf{V}(0) = \mathbf{V}_0,\ \omega(0) = \omega_0. \tag{17}$$

In (12), $dx = dx_1dx_2$, and the *rate-of-strain tensor* $\mathbf{D}(\mathbf{v})$ is given by

$$\mathbf{D}(\mathbf{v}) = \frac{1}{2}(\nabla\mathbf{v} + \nabla\mathbf{v}^t), \tag{18}$$

and we have, for $G(t)(= G)$ in (15),

$$G(t) = G_0 + \int_0^t \mathbf{V}(s)ds. \tag{19}$$

4. A fictitious domain formulation

The *fictitious domain method* discussed below, offers an alternative to the *ALE* methods investigated in [9], [14], [13]. The basic idea is quite simple and can be summarized as follows:

(i) *Fill each particle with the surrounding fluid.*
(ii) *Impose a rigid body motion to the fluid inside each particle.*

(iii) *Relax the rigid body motion inside each particle by using a distributed Lagrange multiplier defined over the space region occupied by the particles.*

In the following, we shall assume that B is made of an homogeneous material of density ρ_s. Starting from the global variational formulation (12)-(17) and following steps (i) to (iii) leads to the following *generalized variational problem*, where $\boldsymbol{\lambda}(t)$ is the *distributed Lagrange multiplier* forcing at time t rigid body motion for the fluid "filling" body B:

$$\begin{aligned} &Find\ \mathbf{U}(t) \in W_{g_0(t)} = \{\mathbf{v} | \mathbf{v} \in H^1(\Omega)^2,\ \mathbf{v} = \mathbf{g}_0(t)\ on\ \Gamma\},\\ &P(t) \in L^2_0(\Omega) = \{q | q \in L^2(\Omega),\ \int_\Omega q dx = 0\},\\ &\boldsymbol{\lambda}(t) \in \Lambda(t) = L^2(B(t))^2\ or \boldsymbol{\lambda}(t) = H^1(B(t))^2,\ so\ that \end{aligned}$$

$$(20)\quad \begin{cases} \rho_f \int_\Omega \frac{\partial \mathbf{u}}{\partial t} \cdot \mathbf{v} dx + \rho_f \int_\Omega (\mathbf{U} \cdot \nabla)\mathbf{U} \cdot \mathbf{v} dx - \int_\Omega P \nabla \cdot \mathbf{v} dx \\ +2\nu_f \int_\Omega \mathbf{D}(\mathbf{U}) : \mathbf{D}(\mathbf{v}) dx + (1 - \rho_f/\rho_s) M(\dot{\mathbf{V}} - \mathbf{g}) \cdot \mathbf{Y} \\ +(1 - \rho_f/\rho_s) I\dot{\omega}\theta - < \boldsymbol{\lambda}, \mathbf{v} - \mathbf{Y} - \boldsymbol{\theta} \times \vec{Gx} >_{B(t)} = \rho_f \int_\Omega \mathbf{g} \cdot \mathbf{v} dx, \\ \forall \mathbf{v} \in H^1_0(\Omega)^2,\ \forall \{\mathbf{Y}, \theta\} \in I\!R^3, \end{cases}$$

$$(21)\quad \int_\Omega q \nabla \cdot \mathbf{U} dx = 0,\ \forall q \in L^2(\Omega),$$

$$(22)\quad < \boldsymbol{\mu}, \mathbf{U} - \mathbf{V} - \boldsymbol{\omega} \times \vec{Gx} >_{B(t)} = 0,\ \forall \boldsymbol{\mu} \in \Lambda(t),$$

$$(23)\quad \mathbf{U} = \mathbf{g}_0\ on\ \Gamma,$$

$$(24)\quad \mathbf{U}(x,0) = \mathbf{U}_0(x), x \in \Omega,\ with\ \nabla \cdot \mathbf{U}_0 = 0\ and\ \mathbf{U}_0|_{\Omega \setminus \overline{B(0)}} = \mathbf{u}_0,$$

$$(25)\quad \mathbf{V}(0) = \mathbf{V}_0,\ \omega(0) = \omega_0, G(0) = G_0.$$

If (20)-(25) hold, it can be easily shown that $\mathbf{U}(t)|_{\Omega \setminus \overline{B(t)}} = \mathbf{u}(t)$, $P(t)|_{\Omega \setminus \overline{B(t)}} = p(t)$, where $\{\mathbf{u}(t), p(t)\}$ completed by $\{\mathbf{V}(t), \omega(t)\}$ is a solution of the global variational problem (12)-(17). The above formulation deserves several remarks; we shall limit ourselves to

REMARK 1. From a *mathematical* point of view, the good choice for $\Lambda(t)$ is $H^1(B(t))^2$ with $< \cdot, \cdot >_{B(t)}$ defined by either

$$(26)\quad < \boldsymbol{\mu}, \mathbf{v} >_{B(t)} = \int_{B(t)} (\boldsymbol{\mu} \cdot \mathbf{v} + d^2 \nabla \boldsymbol{\mu} : \nabla \mathbf{v}) dx,$$

or

$$(27)\quad < \boldsymbol{\mu}, \mathbf{v} >_{B(t)} = \int_{B(t)} (\boldsymbol{\mu} \cdot \mathbf{v} + d^2 \mathbf{D}(\boldsymbol{\mu}) : \mathbf{D}(\mathbf{v})) dx,$$

where, in (26) and (27), d^2 is a *scaling factor*, with d a *characteristic length*, an obvious choice for d being the *diameter* of B. An obvious advantage of $< \cdot, \cdot >_{B(t)}$ defined by (27) is that the differential part of it vanishes if $\mathbf{v}$ is a rigid body motion velocity field.

The choice $\Lambda(t) = L^2(B(t))^2$ is not suitable for the continuous problem, since, in general, $\mathbf{u}$ and P do not have enough regularity for $\boldsymbol{\lambda}$ to be in $L^2(B(t))^2$. On the other hand, $< \cdot, \cdot >_{B(t)}$ defined by

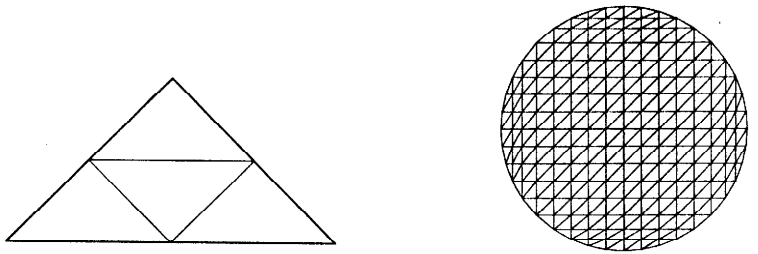

FIGURE 2. Refinement of a triangle of $\mathcal{T}^\Omega_{2h}$ (left) and a triangulation of a disk (right).

$$(28)\quad < \boldsymbol{\mu}, \mathbf{v} >_{B(t)} = \int_\Omega \boldsymbol{\mu} \cdot \mathbf{v} dx$$

makes sense for the *finite dimensional approximations* of problem (20)-(25), in order to force rigid body motion inside B.

REMARK 2. In the case of *Dirichlet boundary conditions* on Γ, and taking the *incompressibility condition* $\nabla \cdot \mathbf{U} = 0$ into account, we can easily show that

$$(29)\quad 2\nu_f \int_\Omega \mathbf{D}(\mathbf{U}) : \mathbf{D}(\mathbf{v}) dx = \nu_f \int_\Omega \nabla \mathbf{U} : \nabla \mathbf{v} dx,\ \forall \mathbf{v} \in W_0,$$

which, from a *computational* point of view, leads to a substantial simplification in (20)-(25).

REMARK 3. The distributed Lagrange multiplier approach can be applied to the cases where the particles have different densities and/or shapes. We are currently investigating the extension of this approach to visco-elastic fluid flow.

REMARK 4. The distributed Lagrange multiplier approach discussed here takes full advantage of the particle rigidity. For deformable particles, we can not apply the above method, directly at least.

Further remarks and comments can be found in [6].

5. Finite element approximation of problem (20)-(25)

5.1. Generalities. Concerning the *space approximation* of problem (20)-(25) the main *computational* issues are:

(i) The approximation of $\mathbf{U}$ and P which are functions defined over Ω.
(ii) The approximation of the multiplier $\boldsymbol{\lambda}$, which is defined over the *moving* domain $B(t)$.
(iii) The approximation of the *bilinear* functional

$$\{\boldsymbol{\mu}, \mathbf{v}\} \rightarrow < \boldsymbol{\mu}, \mathbf{v} >_{B(t)}.$$

The most delicate issue is (iii).

5.2. On the pressure and velocity spaces. In the following, we shall denote by h the pair $\{h_\Omega, h_B\}$, where h_Ω and h_B are space discretization steps associated to *finite element approximations* defined over Ω and B, respectively. Assuming that $\Omega(\subset I\!R^2)$ is polygonal (as in Figure 1), we introduce a *finite element triangulation* $\mathcal{T}_{2h}^{\Omega}$ of Ω, so that $\cup_{T\in\mathcal{T}_{2h}^{\Omega}} T = \overline{\Omega}$, and then a twice finer triangulation $\mathcal{T}_h^{\Omega}$ obtained by joining the mid-points of the edges of the triangles of $\mathcal{T}_{2h}^{\Omega}$, as shown in Figure 2, above.

The *pressure spaces* $L^2(\Omega)$ and $L_0^2(\Omega)$ are approximated by

$$L_h^2 = \{q_h | q_h \in C^0(\bar{\Omega}),\ q_h|_T \in P_1,\ \forall T \in \mathcal{T}_{2h}^{\Omega}\}, \tag{30}$$

$$L_{0h}^2 = \{q_h | q_h \in L_h^2,\ \int_\Omega q_h dx = 0\}, \tag{31}$$

respectively, with P_1 the space of the polynomials of two variables of degree ≤ 1. Similarly, we approximate the velocity spaces W_{g_0} and $W_0(= H_0^1(\Omega)^2)$ by

$$W_{g_0h} = \{\mathbf{v}_h | \mathbf{v}_h \in C^0(\bar{\Omega})^2, \mathbf{v}_h|_T \in P_1^2,\ \forall T \in \mathcal{T}_h^{\Omega},\ \mathbf{v}_h|_T = \mathbf{g}_{0h}\}, \tag{32}$$

$$W_{0h} = \{\mathbf{v}_h | \mathbf{v}_h \in C^0(\bar{\Omega})^2,\ \mathbf{v}_h|_T \in P_1^2,\ \forall T \in \mathcal{T}_h^{\Omega},\ \mathbf{v}_h|_T = \mathbf{0}\}, \tag{33}$$

respectively; in (32), $\mathbf{g}_{0h}$ is an approximation of $\mathbf{g}_0$ so that $\int_\Gamma \mathbf{g}_{0h} \cdot \mathbf{n} d\Gamma = 0$.

The above pressure and velocity finite element spaces - and their 3-D generalizations - are classical ones, concerning the approximation of the Navier-Stokes equations for incompressible viscous fluids (see, e.g., [3] and the references therein for details.)

5.3. Approximation of the multiplier space $\Lambda(t)$. At time t, we approximate the *multiplier space* $\Lambda(t)$ by

$$\Lambda_h(t) = \{\boldsymbol{\mu}_h | \boldsymbol{\mu}_h \in C^0(\bar{B}_h(t))^2, \boldsymbol{\mu}_h|_T \in P_1^2,\ \forall T \in \mathcal{T}_h^{B(t)}\}, \tag{34}$$

where, in (34), $B_h(t)$ is a *polygonal* approximation of $B(t)$ and $\mathcal{T}_h^{B(t)}$ is a triangulation of $B_h(t)$. If $B(t)$ is a *disk*, we take advantage of its *rotation-invariance* by taking for $\mathcal{T}_h^{B(t)}$ the triangulation obtained by translating $\mathcal{T}_h^{B(0)}$ by the vector $\overrightarrow{G_0G(t)}$($\mathcal{T}_h^{B(0)}$ can be viewed as a triangulation of reference); such a triangulation $\mathcal{T}_h^{B(t)}$ is shown in Figure 2.

If $B(t)$ is *not* a disk, we shall take for $\mathcal{T}_h^{B(t)}$ a triangulation *rigidly* attached to $B(t)$.

5.4. Approximation of the bilinear functional $< \cdot, \cdot >_{B(t)}$. Compatibility conditions between h_Ω and h_B. Suppose that the bilinear functional $< \cdot, \cdot >_{B(t)}$ is defined by

$$< \boldsymbol{\mu}, \mathbf{v} >_{B(t)} = \int_{B(t)} (a\boldsymbol{\mu} \cdot \mathbf{v} + b\nabla\boldsymbol{\mu} : \nabla\mathbf{v}) dx,$$

with $a > 0$ and $b \geq 0$. In order to avoid solving complicated mesh intersection problems between $\mathcal{T}_h^{\Omega}$ and $\mathcal{T}_h^{B(t)}$ we approximate $< \cdot, \cdot >_{B(t)}$ (and, in fact $< \cdot, \cdot >_{B_h(t)}$) by

$$\{\boldsymbol{\mu}_h, \mathbf{v}_h\} \rightarrow \int_{B_h(t)} [a\boldsymbol{\mu}_h \cdot (\pi_h\mathbf{v}_h) + b\nabla\boldsymbol{\mu}_h : \nabla(\pi_h\mathbf{v}_h)] dx, \tag{35}$$

where, in (35), π_h is the *piecewise linear interpolation* operator which to $\mathbf{v}_h$ associates the *unique* element of $\Lambda_h(t)$ obtained by interpolating linearly $\mathbf{v}_h$ on the triangles of $\mathcal{T}_h^{B(t)}$, from the values it takes at the vertices of the above triangulation.

As can be expected with mixed variational formulations, some compatibility conditions have to be satisfied between the spaces used to approximate $\{\mathbf{U}, P\}$ and $\boldsymbol{\lambda}$ (see, e.g., [2], [15] for generalities on the approximation of mixed variational problems and several applications). Concerning the particular problem discussed here, namely (20)-(25), let us say that:

(i) *condition $h_B << h_\Omega$ is good to force accurately rigid body motion on $\overline{B(t)}$.*
(ii) *condition $h_\Omega << h_B$ is good for stability.*

Our numerical experiments show that $h_\Omega \simeq h_B$ seems to be the right compromise.

REMARK 5. We can also use collocation methods to force rigid body motion on $\overline{B(t)}$. This approach (inspired from [1]) has been tested and the corresponding results are reported in [6].

5.5. Finite Element approximation of problem (20)-(25). It follows from previous Sections that a quite natural finite element approximation for the mixed variational problem (20)-(25) is the one defined by

Find $\{\mathbf{U}_h, P_h\} \in W_{g_{0h}(t)} \times L_0^2(\Omega)$, $\{\mathbf{V}(t), \omega(t)\} \in I\!R^3$, $\boldsymbol{\lambda}_h(t) \in \Lambda_h(t)$ *so that*

$$\begin{cases} \rho_f \int_\Omega \dfrac{\partial \mathbf{U}_h}{\partial t} \cdot \mathbf{v} dx + \rho_f \int_\Omega (\mathbf{U}_h \cdot \nabla)\mathbf{U}_h \cdot \mathbf{v} dx - \int_\Omega P_h \nabla \cdot \mathbf{v} dx \\ +\nu_f \int_\Omega \nabla\mathbf{U}_h : \nabla\mathbf{v} dx + (1 - \rho_f/\rho_s) M \dfrac{d\mathbf{V}}{dt} \cdot \mathbf{Y} + (1 - \rho_f/\rho_s) I \dfrac{d\omega}{dt}\theta \\ - < \boldsymbol{\lambda}_h, \pi_h\mathbf{v} - \mathbf{Y} - \boldsymbol{\theta} \times \vec{Gx} >_{B_h(t)} = \rho_f \int_\Omega \mathbf{g} \cdot \mathbf{v} dx \\ +(1 - \rho_f/\rho_s) M\mathbf{g} \cdot \mathbf{Y},\ \forall \mathbf{v} \in W_{0h},\ \forall \{\mathbf{Y}, \theta\} \in I\!R^3,\ a.e.,\ t > 0, \end{cases} \tag{36}$$

$$\int_\Omega q \nabla \cdot \mathbf{U}_h dx = 0,\ \forall q \in L_h^2, \tag{37}$$

$$< \boldsymbol{\mu}, \pi_h\mathbf{U}_h - \mathbf{V} - \boldsymbol{\omega} \times \vec{Gx} >_{B_h(t)} = 0,\ \forall \boldsymbol{\mu} \in \Lambda_h(t), \tag{38}$$

$$\mathbf{U}_h(0) = \mathbf{U}_{0h}(\mathbf{U}_{0h} \sim \mathbf{U}_0),\ with \int_\Omega q \nabla \cdot \mathbf{U}_{0h} dx = 0,\ \forall q \in L_h^2, \tag{39}$$

$$\mathbf{V}(0) = \mathbf{V}_0,\ \omega(0) = \omega_0,\ G(0) = G_0, \tag{40}$$

with $G(t) = G_0 + \int_0^t \mathbf{V}(s) ds$.

6. Time discretization by operator-splitting

6.1. Generalities. Most modern *Navier-Stokes* solvers are based on *Operator-Splitting schemes*, in order to force $\nabla \cdot \mathbf{u} = 0$ via a *Stokes solver* (like in, e.g., [3]) or a *L^2-projection method*, (like in, e.g., [16]). This approach applies also to the particulate flow problems discussed here. Indeed, these problems contain three basic computational difficulties, namely:

(i) The *incompressibility condition* $\nabla \cdot \mathbf{U} = 0$ and the related unknown pressure P.
(ii) *Advection* and *diffusion* operators.
(iii) The *rigid body motion* of $B(t)$ and the related *Lagrange multiplier* $\boldsymbol{\lambda}(t)$.

To each of the above difficulties is associated a specific operator; the operators associated to (i) and (iii) are essentially *projection operators.* From an abstract point of view, the problems to be solved (*continuous* or *discrete*) have the following structure:

$$\begin{cases} \dfrac{d\varphi}{dt} + A_1(\varphi,t) + A_2(\varphi,t) + A_3(\varphi,t) = f, \\ \varphi(0) = \varphi_0. \end{cases} \tag{41}$$

To solve (41) we suggest a *fractional-step à la Marchuk-Yanenko* (see [**11**] and the references therein); these schemes are *first order accurate* only, but very stable and easy to implement; actually they can be made second order accurate by *symmetrization.* Applying the Marchuk-Yanenko scheme to the initial value problem, we obtain (with $\Delta t(>0)$ a time discretization step):

$$\varphi^0 = \varphi_0, \tag{42}$$

and for $n \geq 0$, *we compute* φ^{n+1} *from* φ^n *via*

$$\frac{\varphi^{n+j/3} - \varphi^{n+(j-1)/3}}{\Delta t} + Aj(\varphi^{n+j/3}, (n+1)\Delta t) = f_j^{n+1}, \tag{43}$$

for $j = 1,2,3$, *with* $\sum_{j=1}^{3} f_j^{n+1} = f^{n+1}$.

6.2. Application of the Marchuk-Yanenko scheme to particulate flow. With α, β so that $\alpha + \beta = 1$, $0 \leq \alpha, \beta \leq 1$, we *time-discretize* (36)-(40) as follows (the notation is self-explanatory):

$$\mathbf{U}^0 = \mathbf{U}_{0h}, \mathbf{V}^0, \omega^0, G^0 \text{ are given;} \tag{44}$$

for $n \geq 0$, *assuming that* $\mathbf{U}^n, \mathbf{V}^n, \omega^n, G^n$ *are known, solve*

$$\begin{cases} \rho_f \displaystyle\int_\Omega \frac{\mathbf{U}^{n+1/3} - \mathbf{U}^n}{\Delta t} \cdot \mathbf{v} dx - \int_\Omega P^{n+1/3} \nabla \cdot \mathbf{v} dx = 0, \ \forall \mathbf{v} \in W_{0h}, \\ \displaystyle\int_\Omega q \nabla \cdot \mathbf{U}^{n+1/3} dx = 0, \ \forall q \in L_h^2; \ \{\mathbf{U}^{n+1/3}, P^{n+1/3}\} \in W_{g_{0h}}^{n+1} \times L_{0h}^2. \end{cases} \tag{45}$$

Next, compute $\mathbf{U}^{n+2/3}, \mathbf{V}^{n+2/3}, G^{n+2/3}$ *via the solution of*

$$\begin{cases} \rho_f \displaystyle\int_\Omega \frac{\mathbf{U}^{n+2/3} - \mathbf{U}^{n+1/3}}{\Delta t} \cdot \mathbf{v} dx + \alpha \nu_f \int_\Omega \nabla \mathbf{U}^{n+2/3} \cdot \nabla \mathbf{v} dx + \\ \rho_f \displaystyle\int_\Omega (\mathbf{U}^{n+1/3} \cdot \nabla) \mathbf{U}^{n+2/3} \cdot \mathbf{v} dx = \rho_f \int_\Omega \mathbf{g} \cdot \mathbf{v} dx, \\ \forall \mathbf{v} \in W_{0h}; \ \mathbf{U}^{n+1/3} \in W_{g_{0h}}^{n+1}, \end{cases} \tag{46}$$

and

$$\mathbf{V}^{n+2/3} = \mathbf{V}^n + \mathbf{g}\Delta t, \ G^{n+2/3} = G^n + (\mathbf{V}^n + \mathbf{V}^{n+2/3})\Delta t/2. \tag{47}$$

Finally, compute $\mathbf{U}^{n+1}, \boldsymbol{\lambda}^{n+1}, \mathbf{V}^{n+1}, \omega^{n+1}, G^{n+1}$ *via the solution of*

$$\begin{cases} \rho_f \displaystyle\int_\Omega \frac{\mathbf{U}^{n+1} - \mathbf{U}^{n+2/3}}{\Delta t} \cdot \mathbf{v} dx + \beta \nu_f \int_\Omega \nabla \mathbf{U}^{n+1} \cdot \nabla \mathbf{v} dx + \\ (1 - \rho_f/\rho_s) \left(I \dfrac{\omega^{n+1} - \omega^n}{\Delta t} \theta + M \dfrac{\mathbf{V}^{n+1} - \mathbf{V}^{n+2/3}}{\Delta t} \cdot \mathbf{Y} \right) = \\ < \boldsymbol{\lambda}^{n+1}, \pi_h \mathbf{v} - \mathbf{Y} - \boldsymbol{\theta} \times \overrightarrow{G^{n+2/3} x} >_{B_h^{n+2/3}}, \ \forall \mathbf{v} \in W_{0h}, \{\mathbf{Y}, \theta\} \in I\!R^3, \\ < \boldsymbol{\mu}, \pi_h \mathbf{U}^{n+1} - \mathbf{V}^{n+1} - \boldsymbol{\omega} \times \overrightarrow{G^{n+2/3} x} >_{B_h^{n+2/3}} = 0, \ \forall \boldsymbol{\mu} \in \Lambda_h^{n+2/3}, \\ \mathbf{U}^{n+1} \in W_{g_{0h}}^{n+1}, \boldsymbol{\lambda}^{n+1} \in \Lambda_h^{n+2/3}, \mathbf{V}^{n+1} \in I\!R^2, \ \omega^{n+1} \in I\!R, \end{cases} \tag{48}$$

and

$$G^{n+1} = G^n + (V^n + V^{n+1})\Delta t/2. \tag{49}$$

Solving problem (45) is *equivalent* to computing the $L^2(\Omega)$-*projection* of $\mathbf{U}^n$ on the space $W_{g_{0h}}^{n+1}$. This can be done easily using an *Uzawa/conjugate gradient algorithm*, preconditioned by the discrete analogue of $-\nabla^2$ for the *homogeneous Neumann boundary condition*; such an algorithm is described in [**16**]. Problem (46) is a *discrete advection-diffusion problem*; it can be solved by the methods discussed in [**3**].

Finally, problem (48) has the following - classical - *saddle-point* structure

$$\begin{cases} Ax + By = b, \\ B^t x = c, \end{cases} \tag{50}$$

with A a *symmetric* and *positive definite matrix.* Problem (48) can also be solved by an *Uzawa/conjugate gradient* algorithm; such an algorithm is described in [**4**] and [**6**].

7. Remarks on the computational treatment of particle collisions

In the above sections, we have consider the particular case of a *single particle* moving in a region Ω filled with a Newtonian incompressible viscous fluid; we have implicitly discarded possible boundary/particle collisions. The above methodology can be generalized fairly easily to *many particles* cases, with, however, a computational difficulty: one has to prevent particle interpenetration or particle/boundary penetration. To achieve those goals we have included in the *Newton's equations* (6)-(8) modeling particle motions a *short range repulsing force.* If we consider the particular case of *circular* particles (in 2-D) or *spherical* particles in (3-D), and if P_i and P_j are such two particles, with radiuses R_i and R_j and centers of mass G_i and G_j, we shall require the *repulsion force* $\vec{F}_{ij}$ between P_i and P_j to satisfy the following properties:

(i) To be parallel to $\overrightarrow{G_i G_j}$.

(ii) To verify

$$\begin{cases} |\vec{F}_{ij}| = 0 \ if \ d_{ij} \geq R_i + R_j + \rho, \\ |\vec{F}_{ij}| = c/\varepsilon \ if \ d_{ij} = R_i + R_j, \end{cases}$$

with $dij = |\overrightarrow{G_i G_j}|$, c a *scaling factor* and ε *a "small" positive number.*

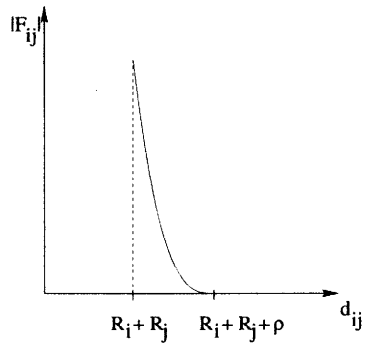

FIGURE 3. Repulsion force behavior

(iii) $|\vec{F_{ij}}|$ has to behave as in Figure 3 for

$$R_i + R_j \leq d_{ij} \leq R_i + R_j + \rho.$$

Parameter ρ is the *range* of the repulsion force; for the simulations discussed in the following Section we have taken $\rho \simeq h_\Omega$.

Boundary/particle collisions can be treated in a similar way (see [**6**] for details).

REMARK 6. The above collision model is fairly simple and is inspired from *penalty techniques* classically used for the computational treatment of some *contact problems* in Mechanics (see, e.g., [**10**], [**5**] for details and applications). Despite its simplicity, this model produces good results, the main reason for that being, in our opinion, that if the fluid is sufficiently viscous and if the fluid and particle densities are close, the collisions - if they occur - are *non violent* ones, implying that the particles which are going to collide move at almost the same velocity just before collision. For more sophisticated models allowing more violent collisions see, e.g., [**12**] and the references therein.

8. Numerical experiments

8.1. 2 particles case. In order to validate the methodology described in the previous sections, we are going to consider a well-documented case, namely the simulation of the motion of 2 circular particles sedimenting in a two-dimensional channel. We shall apply algorithm (44)-(49) with different mesh sizes and time steps. The computational domain is a finite portion of a channel, which is moving along with the particles. Its x and y dimensions are 2 and 5, respectively. The diameter d of the particles is 0.25. The fluid and particle densities are $\rho_f = 1.0$ and $\rho_s = 1.01$, respectively, and the fluid viscosity is $\nu_f = 0.01$. The initial positions of the two circular particles are at the centerline of the channel with distance 0.5 apart. Initial velocity and angular speed of particles are zero. We suppose that at $t = 0$ the flow is at rest.

For numerical simulations, we have chosen two time steps, $\Delta t = 0.0005$ and 0.00025, and two mesh sizes for the velocity field, $h_v = 1/192$ and $1/256$. The mesh size for pressure is always $h_p = 2h_v$. The force range, ρ, in which the short range repulsion force is active is $1.5h_v$. For the (stiffness) parameter, ϵ, mentioned in

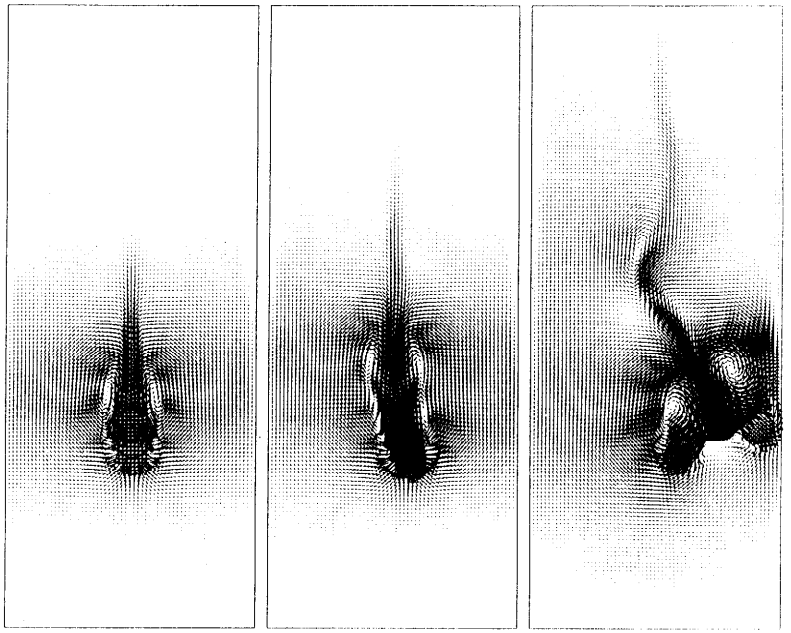

FIGURE 4. Particle position at $t = 0.15$, 0.2, 0.3 (from left to right).

previous Section, we have taken $\epsilon_p = 10^{-5}$ for particle-particle repulsion force and $\epsilon_w = \epsilon_p/2$ for particle-wall repulsion force.

In Figure 4, we can see the fundamental features of two fluidizing particles, i.e., drafting, kissing and tumbling obtained with mesh size $h_v = 1/256$ and time step $\Delta t = 0.0005$. In Figures 5–7, the center of the particles, translation velocity of the center of the particles, and the angular speed of the particles are shown for the cases where the time step is the same, $\Delta t = 0.0005$, and the mesh sizes are $h_v = 1/192$ and $1/256$. The maximal Reynolds numbers in the numerical simulations is about 450. The time at which the two particles are the closest is $t = 0.1665$ in the above two cases. Actually we have a very good agreement between these two simulations until kissing. After kissing, despite the stability breaking which is clearly the manifestation of some instability phenomenon, the simulated particle motions are still very close taking into consideration the difficulty of the problem.

Also in Figures 8–10, similar history graphs are shown which are obtained from the same mesh size, $h_v = 1/192$, and two time steps, $\Delta t = 0.0005$ and 0.00025. When the time step is $\Delta t = 0.00025$, the maximal Reynolds number in the numerical simulation is about 465 and the time of the smallest distance occurrence is at $t = 0.17125$. We can also find a very good agreement between these two cases until the kissing occurrence.

These results compare qualitatively well with those of Hu, Joseph, and Crochet in [**8**], which were obtained with different physical parameters and a different numerical methodology.

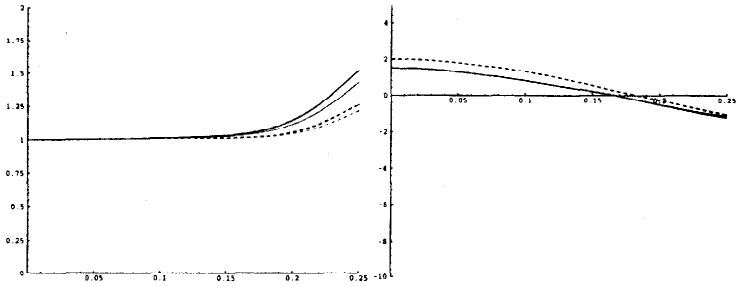

FIGURE 5. History of the x-coordinate (left) and the y-coordinate (right) of the centers of 2 circular particles obtained from different mesh sizes, $h_v = 1/192$ (thick lines) and $h_v = 1/256$ (thin lines).

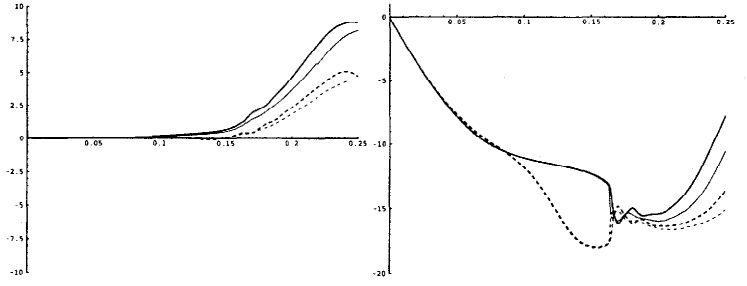

FIGURE 6. History of the x-component (left) and the y-component (right) of the translation velocity of 2 circular particles obtained from different mesh sizes, $h_v = 1/192$ (thick lines) and $h_v = 1/256$ (thin lines).

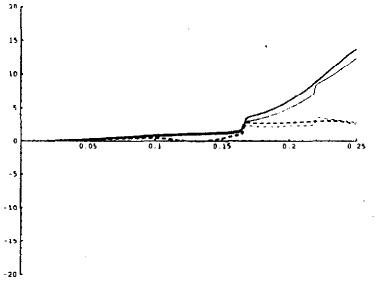

FIGURE 7. History of the angular speed of 2 circular particles obtained from different mesh sizes, $h_v = 1/192$ (thick lines) and $h_v = 1/256$ (thin lines).

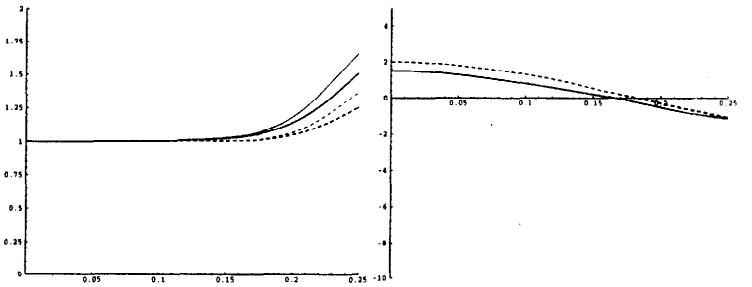

FIGURE 8. History of the x-coordinate (left) and the y-coordinate (right) of the centers of 2 circular particles obtained from different time steps, $\Delta t = 0.0005$ (thick lines) and $\Delta t = 0.00025$ (thin lines).

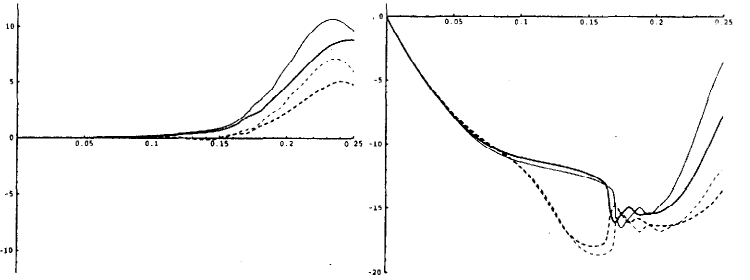

FIGURE 9. History of the x-component (left) and the y-component of the (right) translation velocity of 2 circular particles obtained from different time steps, $\Delta t = 0.0005$ (thick lines) and $\Delta t = 0.00025$ (thin lines).

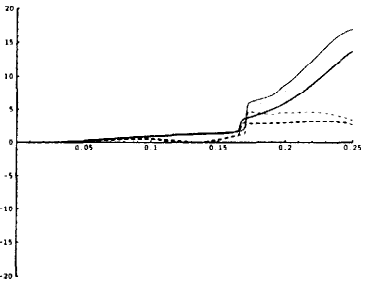

FIGURE 10. History of the angular speed of 2 circular particles obtained from different time steps, $\Delta t = 0.0005$ (thick lines) and $\Delta t = 0.00025$ (thin lines).

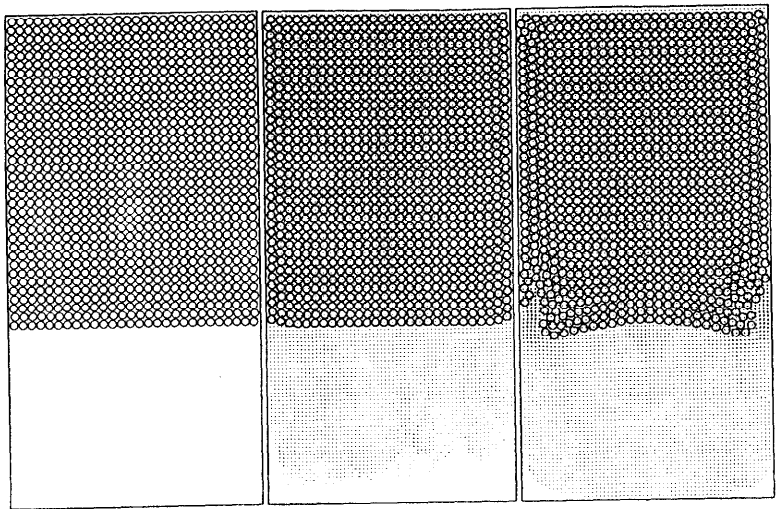

FIGURE 11. Sedimentation of 1008 circular particles: $t = 0$, 1, and 2 (left to right).

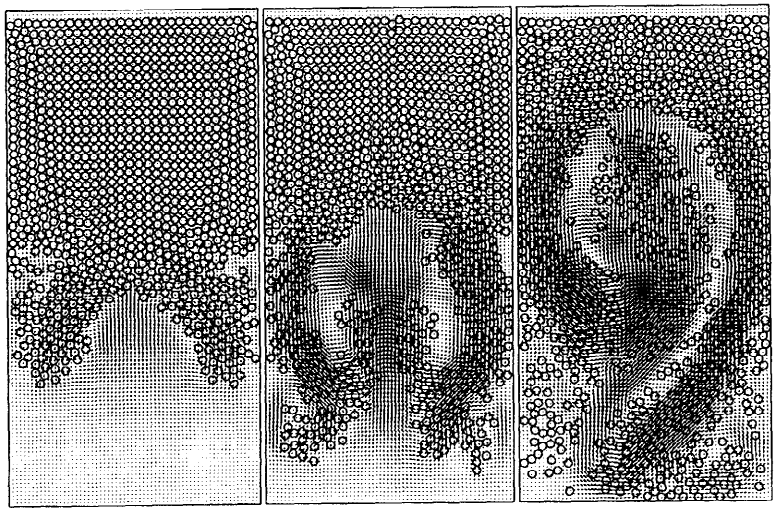

FIGURE 12. Sedimentation of 1008 circular particles: $t = 3$, 4, and 5 (left to right).

8.2. A 1008 particles case. The second test problem that we consider concerns the simulation of the motion of 1008 sedimenting cylinders in the closed channel, $\Omega = (0, 2) \times (0, 4)$. The diameter d of the cylinders is 0.0625 and the position of the cylinders at time $t = 0$ is shown in Figure 11. The solid fraction in this test

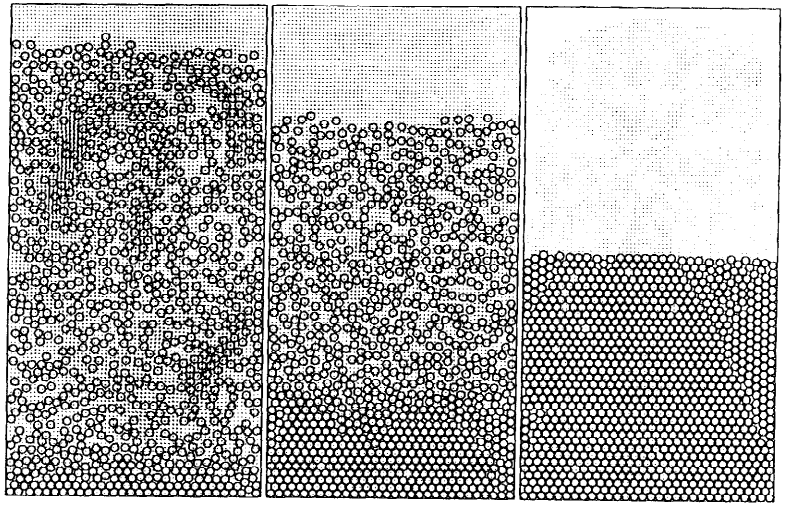

FIGURE 13. Sedimentation of 1008 circular particles: $t = 10$, 20, and 48 (left to right).

case is 38.66%. Initial velocity and angular speed of cylinders are $V_{p,i}^0 = \mathbf{0}$, $\omega_{p,i}^0 = 0$ for $i = 1, \ldots, 1008$. The density of the fluid is $\rho_f = 1.0$ and the density of cylinders is $\rho_s = 1.01$. The viscosity of the fluid is $\nu_f = 0.01$. The initial condition for the fluid flow is $\mathbf{u} = \mathbf{0}$ and $\mathbf{g}_0(t) = \mathbf{0}, \forall t \geq 0$. The time step is $\triangle t = 0.001$. The mesh size for the velocity field is $h_v = 1/256$ (there are 525835 nodes). The mesh size for pressure is $h_p = 1/128$ (131841 nodes). For this many particles case, a fine mesh is required. The parameters for the repulsion force are $\rho = h_v$, $\epsilon_p = 3.26 \times 10^{-5}$, and $\epsilon_w = \epsilon_p/2$. We have chosen $\alpha = 1$ and $\beta = 0$ in the Marchuk-Yanenko scheme. The number of iterations for the divergence free projection problem varies from 12 to 14, the number of iterations for the linearized advection-diffusion problem is 5, and the one for the rigid body motion projection is about 7. Those number of iterations are almost independent of the mesh size and of the number of particles. With the finite dimensional spaces defined in Section 5, the evolution of the 1008 cylinders sedimenting in the closed channel is shown in Figures 11–13. The maximal particle Reynolds number in the entire evolution is 17.44. The slightly wavy shape of the interface observed at t=1 in Figure 11 is a typical onset of a Rayleigh-Taylor instability. When t is between 1 and 2, two small eddies are forming close to the left wall and the right wall and some particles are pulling down fast by these two eddies. Then other two stronger eddies are forming at the lower center of the channel for t between 2 and 4; they push some particles almost to the top wall of the channel. At the end all particles are settled at the bottom of the channel.

8.3. A three dimensional case. The third test problem that we consider here concerns the simulation of the motion of two sedimenting balls in a rectangular cylinder. The initial computational domain is $\Omega = (0, 1) \times (0, 1) \times (-1, 1.5)$, then it moves with the center of the lower ball. The diameter d of two balls is 0.25 and the position of balls at time $t = 0$ is shown in Figure 14. Initial velocity and angular

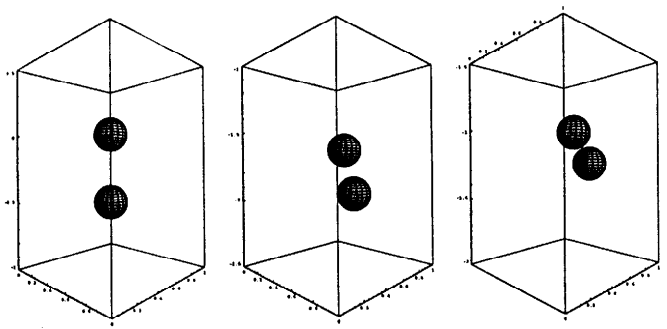

FIGURE 14. Sedimentation of two spherical particles: $t = 0.00$, 0.35, and 0.40 (left to right)

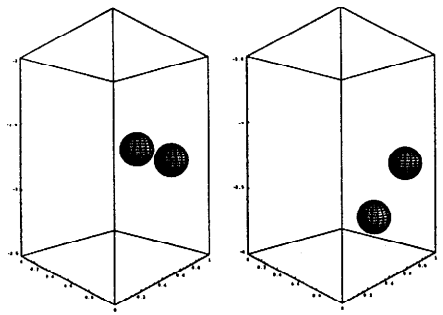

FIGURE 15. Sedimentation of two spherical particles: $t = 0.50$, and 0.70 (left to right)

speed of balls are zero. The density of the fluid is $\rho_f = 1.0$ and the density of balls is $\rho_s = 1.14$. The viscosity of the fluid is $\nu_f = 0.01$. The initial condition for the fluid flow is $\mathbf{u} = \mathbf{0}$ The mesh size for the velocity field is $h_v = 1/40$. The mesh size for pressure is $h_p = 1/20$. The time step is $\Delta t = 0.001$. For the repulsion force parameters, we have now taken, $\rho = h_v$, $\epsilon_p = 8.73 \times 10^{-3}$ and $\epsilon_w = \epsilon_p/2$. The maximal particle Reynolds number in the entire evolution is 198.8. In Figures 14 and 15, we can see the fundamental features of fluidizing two balls, i.e., drafting, kissing and tumbling.

9. Acknowledgments

We acknowledge the helpful comments and suggestions of E. J. Dean, V. Girault, J. He, Y. Kuznetsov, B. Maury, and G. Rodin and also the support of NEC concerning the use of an SX-3 supercomputer. We acknowledge the support of the NSF under HPCC Grand Challenge Grant ECS-9527123, NSF (Grants DMS 8822522, DMS 9112847, DMS 9217374), DRET (Grant 89424), DARPA (Contracts

AFOSR F49620-89-C-0125, AFOSR-90-0334), the Texas Board of Higher Education (Grants 003652156ARP and 003652146ATP) and the University of Houston (PEER grant 1-27682).

References

1. F. Bertrand, P.A. Tanguy, and F. Thibault, *A three-dimensional fictitious domain method for incompressible fluid flow problems*, Int. J. Num. Meth. Fluids **25** (1997), 615–631.
2. F. Brezzi and M. Fortin, *Mixed and hybrid finite element methods*, Springer-Verlag, New York, N.Y., 1991.
3. R. Glowinski, *Numerical methods for nonlinear variational problems*, Springer-Verlag, New York, N.Y., 1984.
4. R. Glowinski, T.I. Hesla, D.D. Joseph, T.W. Pan, and J. Périaux, *Distributed Lagrange multiplier methods for particulate flows*, Computational Science for the 21st Century (M.O. Bristeau, G. Etgen, W. Fitzgibbon, J.L. Lions, J. Périaux, and M.F. Wheeler, eds.), J. Wiley, Chichester, 1997, pp. 270–279.
5. R. Glowinski and P. LeTallec, *Augmented Lagrangian and operator-splitting methods in nonlinear mechanics*, SIAM, Philadelphia, PA, 1989.
6. R. Glowinski, T.W. Pan, T.I. Hesla, D.D. Joseph, and J. Périaux, *A distributed Lagrange multiplier/fictitious domain method for particulate flows*, submitted to *International J. of Multiphase Flow*.
7. T. I. Hesla, *The dynamical simulation of two-dimensional fluid/particle systems*, unpublished notes, 1991.
8. H. H. Hu, D. D. Joseph, and M. J. Crochet, *Direct simulation of fluid particle motions*, Theor. Comp. Fluid Dyn. **3** (1992), 285–306.
9. H.H. Hu, *Direct simulation of flows of solid-liquid mixtures*, Internat. J. Multiphase Flow **22** (1996), 335–352.
10. N. Kikuchi and T.J. Oden, *Contact problems in elasticity*, SIAM, Philadelphia, PA, 1988.
11. G. I. Marchuk, *Splitting and alternate direction methods*, Handbook of Numerical Analysis (P.G. Ciarlet and J.L. Lions, eds.), vol. 1, North-Holland, Amsterdam, 1990, pp. 197–462.
12. B. Maury, *A many-body lubrication model*, C.R. Acad. Sci., Paris, Série I (to appear).
13. B. Maury and R. Glowinski, *Fluid particle flow: a symmetric formulation*, C.R. Acad. Sci., Paris, Série I **t. 324** (1997), 1079–1084.
14. O. Pironneau, J. Liou, and T. Tezduyar, *Characteristic-Galerkin and Galerkin least squares space-time formulations for advection-diffusion equations with time-dependent domains*, Comp. Meth. Appl. Mech. Eng. **16** (1992), 117–141.
15. J.E. Roberts and J.M. Thomas, *Mixed and hybrid methods*, Handbook of Numerical Analysis (P.G. Ciarlet and J.L. Lions, eds.), vol. 2, North-Holland, Amsterdam, 1991, pp. 521–639.
16. S. Turek, *A comparative study of time-stepping techniques for the incompressible navier-stokes equations: from fully implicit non-linear schemes to semi-implicit projection methods*, Int. J. Num. Meth. Fluids **22** (1996), 987–1011.

DEPARTMENT OF MATHEMATICS, UNIVERSITY OF HOUSTON, HOUSTON, TEXAS 77204, USA
E-mail address: roland@math.uh.edu

DEPARTMENT OF MATHEMATICS, UNIVERSITY OF HOUSTON, HOUSTON, TEXAS 77204, USA
E-mail address: pan@math.uh.edu

DEPARTMENT OF AEROSPACE ENGINEERING & MECHANICS, UNIVERSITY OF MINNESOTA, MINNEAPOLIS, MN 55455, USA
E-mail address: hesla@aem.umn.edu

DEPARTMENT OF AEROSPACE ENGINEERING & MECHANICS, UNIVERSITY OF MINNESOTA, MINNEAPOLIS, MN 55455, USA
E-mail address: joseph@aem.umn.edu

DASSAULT AVIATION, 92314 SAINT-CLOUD, FRANCE
E-mail address: periaux@menusin.inria.fr